THERMAL EMITTANCE MEASUREMENTS AT THE SwissFEL INJECTOR TEST FACILITY

E. Prat*, S. Bettoni, H. H. Braun, M. C. Divall, R. Ganter, T. Schietinger, A. Trisorio, C. Vicario
PSI, Villigen, Switzerland
C. P. Hauri, EPFL, Lausanne, Switzerland and PSI, Villigen, Switzerland

Abstract

In a laser-driven RF gun the ultimate limit of the beam emittance is the transverse momentum of the electrons as they exit the cathode, the so-called intrinsic or thermal emittance. In this contribution we present measurements of the thermal emittance at the SwissFEL Injector Test Facility for electron beam charges down to a few tens of fC. We have studied the dependence of thermal emittance and quantum efficiency on the laser wavelength, the RF-gun gradient and the cathode material (copper and cesium telluride).

INTRODUCTION

The electron beam emittance is of great importance for Free-Electron Laser (FEL) facilities. First, transversely coherent FEL radiation is generated if $\varepsilon_n/\gamma \approx \lambda/4\pi$, where ε_n is the normalized beam emittance, γ is the Lorentz factor and λ is the FEL radiation wavelength. This condition entails that by reducing the normalized emittance the final beam energy can be decreased, which translates into a more compact and affordable accelerator. Second, for a given beam energy, a smaller emittance implies a higher radiation power and a shorter undulator beamline to reach FEL saturation.

As accelerator technology advances and the emittance of the electron source is preserved downstream of the injector, the source becomes a significant contributor to the final emittance and brightness of the electron beam. The intrinsic or thermal emittance, which is proportional to the transverse momentum of the electrons exiting the cathode, is related to the initial kinetic energy or effective temperature of the electrons.

The thermal emittance for both metal and semiconductor photo-cathodes can be expressed as [1, 2].

$$\varepsilon_{th} = \sigma_l \sqrt{\frac{\phi_l - \phi_e}{3 m_0 c^2}}, \qquad (1)$$

where ϕ_l is the laser photon energy, σ_l is the RMS laser beam size, m_0c^2 is the electrons rest mass energy, and ϕ_e is the effective work function. We call $\varepsilon_{th}/\sigma_l$ the normalized thermal emittance, expressed in nm/mm, as it is independent of the laser beam size. We note that the above expression is correct if tilted-surface effects related to the surface roughness of the cathode are negligible [3].

To illustrate the effect of the thermal emittance on the final FEL performance, Fig. 1 shows the dependence of the FEL power on the normalized thermal emittance for the 200 pC charge operation mode of SwissFEL [4]. For each normalized thermal emittance value we performed numerical simulations to optimize the emittance at the end of the injector, from which the FEL power was calculated. For instance, the FEL power increases by about 25% for a normalized thermal emittance reduction from 600 nm/mm to 400 nm/mm.

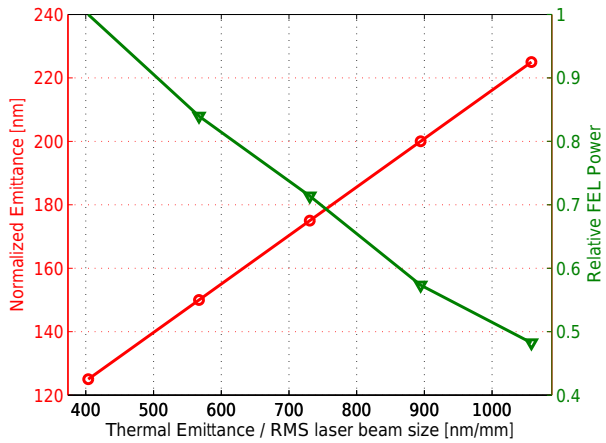

Figure 1: Relative FEL power as function of the normalized thermal emittance. Normalized core slice emittance is simulated for the 200 pC charge operation mode of SwissFEL for different normalized thermal emittance values. The corresponding normalized emittance for optimized laser beam size (red circles) is then used to calculate the relative FEL power (green triangles).

The effective work function is defined as the material work function ϕ_w, reduced by the Schottky effect ϕ_s [5]:

$$\phi_e = \phi_w - \phi_s = \phi_w - \sqrt{\frac{e^3}{4\pi\varepsilon_0}\beta E_c(\varphi)}, \qquad (2)$$

where e is the charge of the electron, ε_0 is the vacuum permittivity, β is the local field enhancement factor that depends on the cathode surface properties, and $E_c(\varphi)$ is the applied field on the cathode at the injection phase φ.

When $E_c(\varphi)$ varies in a small range, the quantum efficiency (QE) of a metal photo-cathode is linked to the laser photon energy and the effective work function as follows [1, 6]:

$$QE \propto (\phi_l - \phi_e)^2. \qquad (3)$$

Equations 2 and 3 allow the determination of the effective work function of the employed cathodes directly from measurements in the RF gun in two independent ways: by measuring the emitted charge as a function of the injection

* eduard.prat@psi.ch

ISBN 978-3-95450-133-5

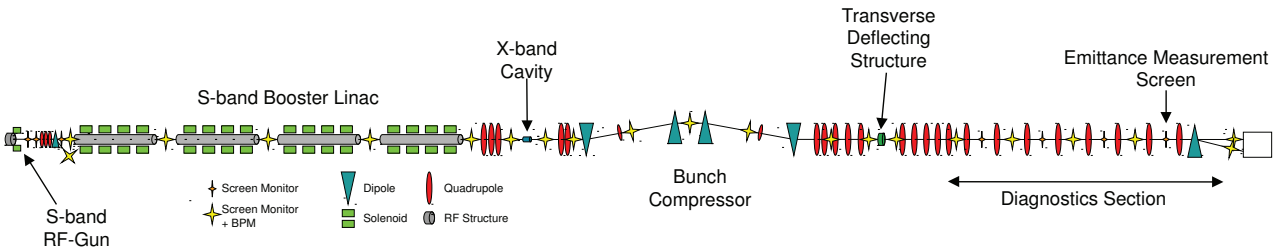

Figure 2: Schematic layout of the SwissFEL Injector Test Facility (not to scale). The total length is about 60 m.

phase (Schottky scan) and as a function of the laser energy (wavelength scan).

Extensive worldwide research and development have been performed in the last years to measure the thermal emittance for metal and semiconductor photo-cathodes, see for example Refs. [6–10]. We have experimentally studied at the SwissFEL Injector Test Facility [11] the normalized thermal emittance and QE dependence on the laser wavelength λ_l ($\phi_l = hc/\lambda_l$), the RF field at the cathode E_c, and the photo-cathode material (related to ϕ_w). These studies are presented for copper and cesium telluride.

We note that most of the results presented in this conference contribution will soon be published in a peer-reviewed journal [12].

THE SwissFEL INJECTOR TEST FACILITY

The SwissFEL Injector Test Facility is the principal test bed and demonstration plant for the SwissFEL project, which is presently under construction and aims at realizing a hard-X-ray FEL by 2017. Figure 2 shows a sketch of the SwissFEL Injector Test Facility.

Electron bunches of charges between 10 pC and 200 pC are generated in a 2.6-cell standing-wave S-band RF photo-injector gun, originally developed for high-current operation at the CLIC test facility (CTF) at CERN [13]. There are two gun drive lasers. The main one is based on a Ti:Sapphire chirped pulse amplification system [14], which allows the variation of the 3rd harmonic emission between 260 and 280 nm. This is further extended by the use of an optical parametric amplifier (OPA) and a conversion stage to 250–310 nm. The second laser system is a compact, turn-key Nd:YLF amplifier, with a fixed wavelength of 262 nm. A longitudinal Gaussian profile of 9.9 ps FWHM is used for the measurements presented here and a selection of different size circular apertures cut the central homogeneous part of the laser beam, which is imaged onto the cathode for each wavelength at close to normal incidence.

The total beam energy at the gun exit is 7.1 MeV. A solenoid close to the gun cavity is used for initial focusing. Additional individually powered windings inside the gun solenoid allow for correction of normal- and skew-quadrupole field components.

Four S-band accelerating structures bring the beam energy up to the nominal value of 250 MeV. Additional solenoid magnets around these structures allow for further control of the transverse optics. After some space, which is used for an X-band linearizing system and a bunch-compressor chicane, an S-band transverse deflecting cavity is used for longitudinally resolved measurements such as bunch length and slice emittance. A dedicated beam diagnostic section downstream of the deflecting cavity allows us to characterize the accelerated beam. Several quadrupole magnets and beam screens measuring the transverse beam profile are available for emittance measurements. The final beam energy is measured by a spectrometer at the end of the diagnostic section.

More details on the SwissFEL Injector Test Facility can be found in Ref. [11].

MEASUREMENT PROCEDURES

When the emittance measurements are performed with sufficiently low charge to avoid space charge effects, the emittance of a selected longitudinal slice of the bunch corresponds to the thermal emittance. In our case we choose the central slices of the bunch, what we call the core slice emittance. The normalized thermal emittance $\varepsilon_{th}/\sigma_l$ can be reconstructed by measuring the thermal emittance as a function of the RMS laser beam size, which is varied by changing the laser aperture.

It is crucial to establish a reliable and high-resolution method to be able to precisely measure the thermal emittance of the electrons. Core slice emittance measurements are performed by streaking the bunch and visualizing it on a high-resolution YAG screen [15] at the high energy section of the machine. We can streak the beam either with a RF transverse deflector or by introducing dispersion to an energy-chirped beam. The normalized emittance resolution is about 2–3 nm for a final beam energy of 250 MeV. The longitudinal resolution is about 13 fs when the transverse deflector is used. With the dispersion method we can resolve more than 5 slices per RMS bunch length (if the RMS energy chirp of the beam is 1%). The statistical and systematic errors of the emittance are estimated to be below the 5% level. A more detailed description of the slice emittance measurements can be found in Refs. [16, 17].

The YAG screen has allowed measurements for bunch charges of 1 pC and less, where space charge effects are negligible for our laser beam sizes. The critical surface charge density in our case is ≈ 30 pC/mm^2 at 50 MV/m field on the cathode with a 9.9 ps FWHM pulse and has been

ISBN 978-3-95450-133-5

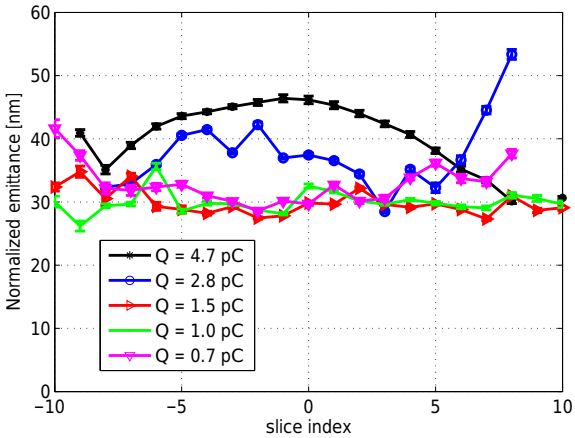

Figure 3: Measured slice emittance as a function of bunch charge to find the space-charge limit. Measurements for a bunch charge of 1 pC and less give the same core slice emittance values within the accuracy of the measurement, while at higher charge the presence of a space charge effect is clearly visible.

identified by reducing the bunch charge at fixed laser beam size until the emittance was no longer reduced, as shown in Figure 3. Once the space-charge limit is found, the charge surface density is kept constant during the aperture scan to avoid space charge effects.

The QE is measured by recording the charge at a calibrated beam position monitor 2.6 m downstream of the gun while changing the laser intensity.

MEASUREMENT RESULTS

We used four cathodes for our measurements, two made of pure copper, labeled $Cath_3$ and $Cath_{19}$, and two coated with cesium telluride labeled $Cath_{13}$ and $Cath_8$. The cesium telluride cathodes are prepared by depositing about 15 nm of tellurium and about 25 nm of cesium on a copper cathode. All the photocathodes were mounted in a load-lock chamber. More details on the cathode preparation can be found in Ref. [18].

We measured the dependence of the thermal emittance on the laser wavelength for the copper cathode $Cath_3$ and the influence of the gun gradient for the copper cathode $Cath_{19}$. The wavelength dependence measurements were carried out with the Ti:Sapphire laser, while all the rest of the measurements presented here were performed with the Nd:YLF laser.

Laser Wavelength

Figure 4 shows the core slice emittance measurements as a function of the laser beam size (aperture scan) for two different wavelengths (260.1 nm and 267.6 nm).

We observed a linear growth of the normalized thermal emittance as a function of the laser beam size (bottom plot of Fig. 4). This is in contradiction with Eq. 1, but can be explained by our present gun design, which exposes the

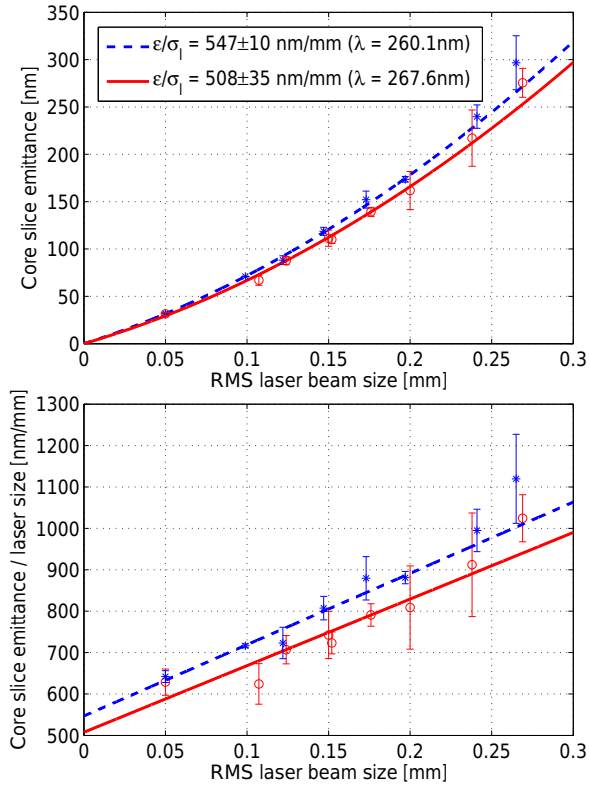

Figure 4: Core slice emittance as a function of the laser beam size for two laser wavelengths — 260.1 nm (dashed blue) and 267.6 nm (red solid) – for cathode $Cath_3$.

electron beam to a quadrupole field component due to non-coaxial RF feeds from opposing sides. Indeed, the inhomogeneity of the cathode was ruled out as an explanation by measuring the core slice emittance at the smallest aperture, while moving the laser beam across the cathode. The non-linear dependence of the asymmetric field in the gun was verified by aperture scans at different gun gradients (see next subsection). Taking the quadratic component into account the normalized thermal emittance can be determined as the extrapolation of the quadratic fit to an infinitely small laser beam size. The normalized thermal emittance corresponds to the linear term of a second-order fit to the emittance data, which gave 547±10 nm/mm for a wavelength of 260.1 nm and 508±35 nm/mm for a wavelength of 267.6 nm.

One month later we performed measurements at four different wavelengths using the same cathode ($Cath_3$). These measurements were realized with a charge of 1 pC and at the smallest laser aperture, corresponding to about 50 µm RMS laser beam size on the cathode. We note that measurements performed with only the smallest aperture overestimate the normalized thermal emittance by 10–20%.

We measured the QE for different laser wavelengths, as shown in Fig. 5. The measurements were taken with the Ti:sapphire and the OPA, covering a wavelength range of 248–301 nm. By using Eq. 3 the best fit found for $Cath_3$ corresponds to an effective work function of 3.93±0.03 eV (see inset of Fig. 5).

ISBN 978-3-95450-133-5

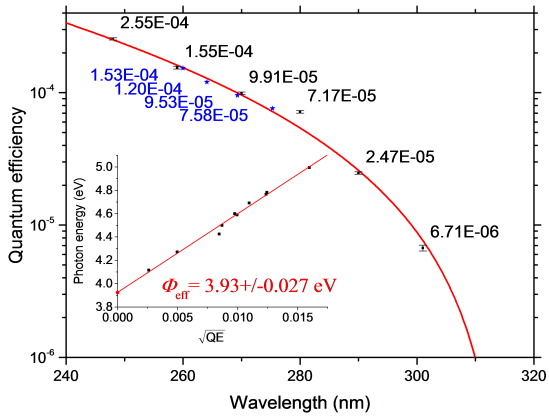

Figure 5: QE as a function of wavelength with cathode $Cath_3$. Measurements were performed with both the OPA (black points) and the 3rd harmonic of the Ti:sapphire laser (blue stars). The fit based on Eq. 3 (inset) gives an effective work function of 3.93 eV (red line).

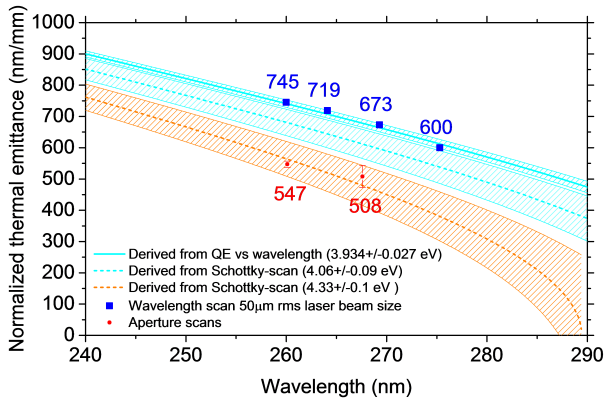

Figure 6: Normalized thermal emittance as a function of wavelength for cathode $Cath_3$. Measurements with the smallest aperture below the space charge limit, at 1 pC (blue squares). Reconstructed thermal emittance calculated from the effective work functions determined from the QE measurements as a function of wavelength shown in Fig. 4 (cyan solid) and from the Schottky measurements (cyan dashed). Two points derived from the aperture scan a month earlier shown on Fig. 4 (red dots) with the reconstruction from the Schottky scan performed at the same time (orange dashed).

Alternatively we estimated the effective work function by performing a Schottky scan, i.e., by measuring the emitted charge as a function of the gun phase. By using Eqs. 2 and 3 and fitting the points around the operational phase, the best fit was found with a work function of 4.56 eV for this cathode, giving an effective work function of 4.06±0.09 eV. This value is close to the one from the wavelength scan. A Schottky scan done at the same time of the measurements shown in Fig. 4 gave an effective work function of 4.33±0.10 eV.

Figure 6 summarizes the thermal emittance measurements performed as a function of the laser wavelength. There is a good agreement between the thermal emittance determined from the core slice emittance measurements and from the wavelength and Schottky scans.

Gun Gradient

Figure 7 shows an aperture scan measurement for the copper cathode $Cath_{19}$ for three different gun gradients corresponding to the following fields on the cathode $E_c(\varphi)$: 49.4 MV/m (nominal value), 34.8 MV/m and 16.4 MV/m. As expected from the RF-induced effect, the quadratic component decreased as a function of the gradient: it was 716±84 nm/mm^2 at 49.9 MV/m, 508±137 nm/mm^2 at 34.8 MV/m, and 321±105 nm/mm^2 at 16.4 MV/m. The fitted normalized thermal emittances diminished for lower field on the cathode, following the dependence indicated in Eqs. 1 and 2: the normalized thermal emittance was 428±16 nm/mm at 49.9 MV/m, 370±25 nm/mm at 34.8 MV/m, and 346±25 nm/mm at 16.4 MV/m.

For the lowest gun gradient it was possible to measure the slice emittance for a total bunch charge of about 30 fC. This was possible thanks to the high sensitivity of our profile monitor and due to the smaller amount of dark current produced by the gun with the lower RF gradient. The measurement for this ultra-low charge is shown in Figure 8. The core slice emittance was below 25 nm. This measurement was done

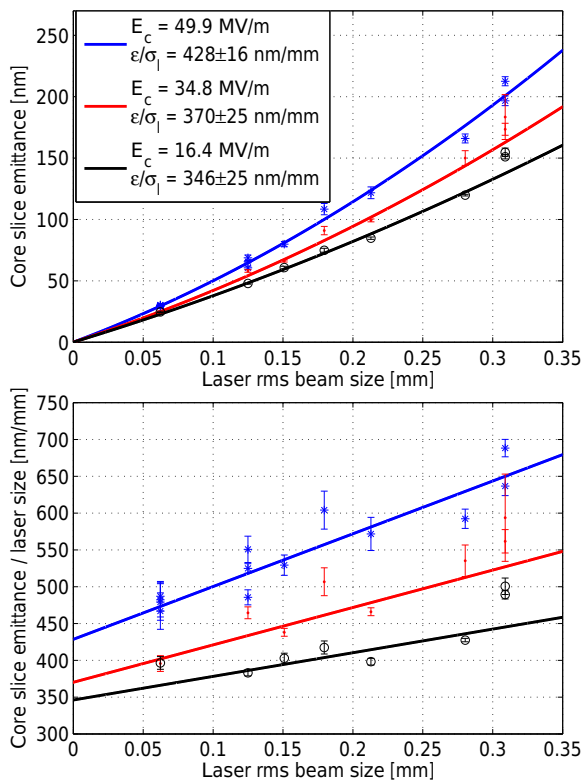

Figure 7: Core slice emittance as a function of beam size for three different fields on the cathode. The nonlinear effect was strongly reduced at lower field and the normalized thermal emittance varied as expected from theory.

ISBN 978-3-95450-133-5

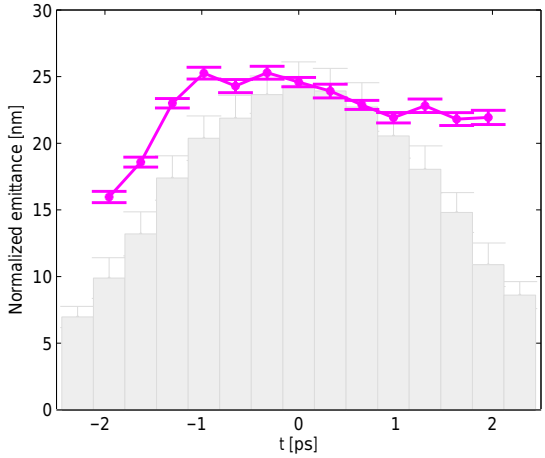

Figure 8: Normalized slice emittance in the horizontal plane for a bunch charge of 30 fC (magenta). The error bars are obtained by error propagation of the statistical beam-size errors. The longitudinal bunch charge profile is shown in gray bars.

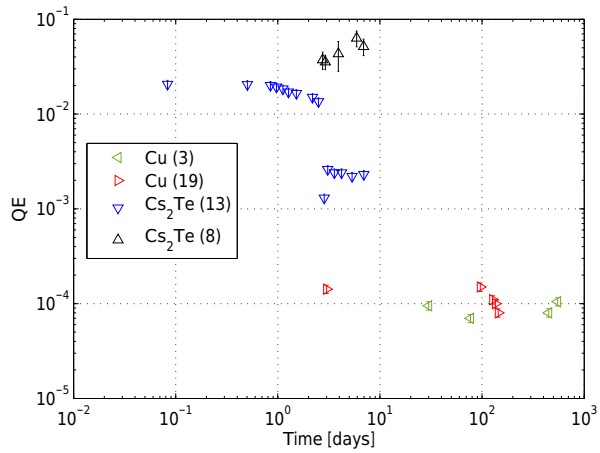

Figure 9: QE evolution of the four photocathodes tested at the SwissFEL Injector Test Facility, two copper ($Cath_3$ and $Cath_{19}$) and two cesium telluride ($Cath_{13}$ and $Cath_8$).

by employing the smallest aperture, corresponding to about 50 µm RMS laser beam size at the cathode.

Cathode Material

We have tested each of the two cesium telluride cathodes for one week of operation. The thermal emittance of both cathodes was measured with aperture scans. For the cesium telluride cathode $Cath_8$ only measurements at the three smallest laser apertures were considered to be valid, due to the inhomogeneities of the QE outside the cathode center. The value of the thermal emittance for the cesium telluride cathodes $Cath_{13}$ and $Cath_8$ was 713±88 nm/mm and 549± 29 nm/mm, respectively. We measured the thermal emittance for the copper cathode $Cath_{19}$ with the same machine conditions as when we performed the measurement with the cesium telluride $Cath_8$. The thermal emittance in this case was 430±20 nm/mm, a value about 25% lower than for cesium telluride.

We have performed, for the two photo-cathode materials (with $Cath_3$ and $Cath_{13}$), an emittance optimization for an electron bunch with a 200 pC beam charge. We have achieved a slice emittance of about 200 nm for copper [16] and of about 250 nm for cesium telluride. Again, the degradation of the emittance when moving from copper to cesium telluride is about 25%.

Figure 9 shows the QE evolution of all the four cathodes tested at the SwissFEL Injector Test Facility. The copper cathodes were operated for several months ($Cath_3$ for about 5 months and $Cath_{19}$ for about 18 months), while the two cesium telluride cathodes ($Cath_{13}$ and $Cath_8$) could be tested only for one week each. The copper cathodes show a stable value of the QE around the 10^{-4} level. Both cesium telluride cathodes provided a QE of about 2% at the beginning of their operation. Whereas on the third day of operation the QE of $Cath_{13}$ suddenly dropped to about 2×10^{-3}, the QE of $Cath_8$ stayed above 2% for the whole week. The reason for the QE deterioration of $Cath_{13}$ is not understood.

For the copper cathodes the QE, measured with the smallest available laser beam size, varied by about 15% across the area of measurements shown here. The cesium telluride cathodes were less homogeneous, with QE changing by up to a factor of two.

CONCLUSION

Table 1 displays all the normalized thermal emittance measurements presented in this contribution. To our knowledge, this is the first time that measurements for copper and cesium telluride are performed under the same conditions and that thermal emittance measurements agree well with theoretical expectations [1, 2]. Moreover, our measured normalized thermal emittances follow the expected dependence on the laser wavelength and field at the cathode: the emittance is smaller for longer wavelengths ($\varepsilon_{th}/\sigma_l \propto \phi_l^{1/2}$) and for reduced field on the cathode ($\varepsilon_{th}/\sigma_l \propto E_c^{1/4}$). We have verified, as suggested by Ref. [1], that a longer wavelength provides a smaller thermal emittance but gives also a lower QE. We have shown that the thermal emittance can be estimated from Schottky scans (charge as a function of the RF phase) or wavelength scans (charge as a function of the laser wavelength).

Cesium telluride provides a QE which is about two orders of magnitude higher than for the standard copper cathodes, while the emittance deterioration is only about 25%. This indicates that cesium telluride could be a viable alternative for SwissFEL. For a firm conclusion, however, more work on improving the surface homogeneity as well as long-term operation tests to evaluate the QE evolution with time are still needed.

For a reduced field at the cathode of 16.4 MV/m we have measured a normalized thermal emittance of about 350 nm/mm. This is, to our knowledge, the smallest normal-

ISBN 978-3-95450-133-5

Table 1: Measured Normalized Thermal Emittances at the SwissFEL Injector Test Facility

Label	Material	Measurement day	Normalized thermal emittance [nm/mm]	Laser wavelength [nm]	Field on the cathode [MV/m]
$Cath_3$	copper	31-10-2012	547±10	260.1	49.9
	copper	30-10-2012	508±35	267.6	49.9
$Cath_{19}$	copper	25-09-2013	428±16	262.0	49.9
	copper	25-09-2013	370±25	262.0	34.8
	copper	27-09-2013	346±25	262.0	16.4
	copper	04-04-2014	430±20	262.0	49.9
$Cath_{13}$	cesium telluride	28-10-2013	713±88	262.0	49.9
$Cath_8$	cesium telluride	04-04-2014	549±29	262.0	49.9

ized thermal emittance ever measured in an accelerator. The experimental verification of such small values was made possible through our reliable, high-resolution measurement procedure.

ACKNOWLEDGMENTS

We would like to thank the Beam Diagnostics team of PSI, in particular Rasmus Ischebeck, for developing and implementing the SwissFEL profile monitor used in our measurements. We acknowledge the extensive contributions of all the other PSI expert groups and the SwissFEL team to the construction and operation of the SwissFEL Injector Test Facility. We finally thank Masamitsu Aiba, Florian Müller, Sven Reiche and Mattia Schär for fruitful discussions that helped to improve the quality of the manuscript.

REFERENCES

[1] D. H. Dowell and J. Schmerge, Phys. Rev. ST Accel. Beams **12**, 074201 (2009).

[2] K. Flöttmann, TESLA FEL Report 1997-01 (1997).

[3] D. H. Dowell, in *Photocathode Physics for Photoinjectors* Workshop, Ithaca, USA (2012).

[4] R. Ganter (ed.), PSI Report 10-04 (2012).

[5] Z. M. Yusof, M. E. Conde, and W. Gai, Phys. Rev. Lett. **93**, 114801 (2004).

[6] H. J. Qian et al., Phys. Rev. ST Accel. Beams **15**, 040102 (2012).

[7] D. Sertore, D. Favia, P. Michelato, L. Monaco, and P. Pierini, Proc. EPAC'04, Lucerne, Switzerland, 408–410 (2004).

[8] Y. Ding et al., Phys. Rev. Lett. **102**, 254801 (2009).

[9] F. Stephan et al., Phys. Rev. ST Accel. Beams **13**, 020704 (2010).

[10] C. P. Hauri et al., Phys. Rev. Lett. **104**, 234802 (2010).

[11] M. Pedrozzi (ed.), PSI Report 10-05 (2010).

[12] M. Divall et al., to be published.

[13] R. Bossart and M. Dehler, Proc. EPAC'96, Sitges, Spain 1544-1546 (1996).

[14] A. Trisorio, P. M. Paul, F. Ple, C. Ruchert, C. Vicario, and C. P. Hauri, Optics Express **19**, 20128 (2011).

[15] R. Ischebeck and E. Prat, to be published.

[16] E. Prat et al., Proc. FEL'13, New York, NY, USA, 200–204 (2013).

[17] E. Prat and M. Aiba, Phys. Rev. ST Accel. Beams **17**, 032801 (2014).

[18] R. Ganter et al., these Proceedings Proc. 36th Int. Free-Electron Laser Conf., Basel, 2014, MOA02

ISBN 978-3-95450-133-5